Twinned or not twinned, that is the question: crystallization and preliminary crystallographic analysis of the ^{2}F1^{3}F1 module pair of human fibronectin

Enrique Rudiño-Piñera,[a,b]*
Ulrich Schwarz-Linek,[a]
Jennifer R. Potts[a] **and**
Elspeth F. Garman[a]*

[a]Department of Biochemistry, University of Oxford, South Parks Road, Oxford OX1 3QU, England, and [b]Departamento de Medicina Molecular y Bioprocesos, Instituto de Biotecnología, Universidad Nacional Autónoma de México, PO Box 510-3, Cuernavaca, MOR 62271, Mexico

Correspondence e-mail:
enrique@biop.ox.ac.uk,
elspeth@biop.ox.ac.uk

Human fibronectin (Fn) is a large multidomain protein found in the extracellular matrix and plasma. It is involved in many cellular processes, including cell adhesion and migration during embryogenesis and wound healing. The ability to bind Fn is a characteristic that has been demonstrated for a number of pathogens. For *Staphylococcus aureus* and *Streptococcus pyogenes* in particular, Fn-binding bacterial proteins (FnBPs) have been shown to mediate not only bacterial adhesion to host cells but also the uptake of bacteria by the cells. FnBPs interact with the amino-terminal region of Fn, where five type I ($^{1-5}$F1) Fn modules are located. Although the structures of two F1 module pairs have been determined by NMR, no X-ray structures have been reported. To explore the conformational interactions between modules and the binding properties of FnBPs, the ^{2}F1^{3}F1 module pair was crystallized using the vapour-diffusion method at 298 K. 12 X-ray diffraction data sets have been collected: six on an in-house rotating anode (three native, one Pt derivative and two peptide-bound) and six at synchrotron-radiation sources (two native and four derivative). Following analysis of these data, some of which have very high multiplicity (up to 50), probable space-group assignments were made ($P42_12$, $P4_12_12$ or $P4_32_12$) and the possibly twinned nature of the crystals was investigated using six different tests. The results presented here suggest that the crystals are not twinned.

1. Introduction

Human fibronectin is an extracellular multidomain glycoprotein that interacts with a variety of macromolecules, including components of the extracellular matrix, plasma proteins and cell-surface receptors (Hynes, 1990). It exists as a soluble dimer (linked by two disulfide bridges) in the plasma and as an insoluble multimer in the extracellular matrix (Hynes, 1990). Fibronectin is mainly composed of three kinds of modules, which are designated F1, F2 and F3 and are separated by connecting sequences (Bork *et al.*, 1996). Each type of module has been shown to fold independently, but interactions between modules are likely to be important for function (Potts & Campbell, 1996).

The amino-terminal region of mature fibronectin is formed by five F1 modules (called ^{1}F1^{2}F1^{3}F1^{4}F1^{5}F1); in sequence, these correspond to residues 1–242. From those, the first 18 residues seem to be non-structured, followed by five F1 modules (^{1}F1, residues 19–59; ^{2}F1, residues 64–107; ^{3}F1, residues 108–151; ^{4}F1, residues 153–197; ^{5}F1, residues 198–242). The consensus fold of the F1 module consists of a double-stranded and a triple-stranded antiparallel β-sheet with two disulfide bridges per module.

Human fibronectin is targeted by bacteria through fibronectin-binding proteins (FnBPs), which are anchored to the bacterial cell wall, and these interactions are likely to play a role in the infection process. For example, FnBP-mediated uptake of bacteria into host cells may aid evasion of the host immune system or administered antibiotics. FnBPs from *Staphylococcus aureus* and *Streptococcus pyogenes* bind to $^{2-5}$F1 or $^{1-5}$F1 from Fn and a novel model for these interactions, a tandem β-zipper, has been proposed (Schwarz-Linek *et al.*, 2003).

The structures of several F1 modules of the fibronectin amino-terminal region have been determined by NMR spectroscopy: ^{7}F1 (Baron *et al.*, 1990), ^{4}F1^{5}F1 (Williams *et al.*, 1994; residues 152–244; PDB code 1fbr), ^{1}F1^{2}F1 (Potts *et al.*, 1999; residues 17–109; PDB code 1qgb), ^{6}F1^{1}F2 (Bocquier *et al.*, 1999; residues 305–405; PDB code 1qo6) and ^{1}F1^{2}F1 in complex with B3, a peptide from FnBB, which is an FnBP from *Streptococcus dysgalactiae* (Schwarz-Linek *et al.*, 2003; PDB code 1o9a). However, no crystallographic structures of any of the F1 modules have been determined,

despite the fact that crystallographic structures of F2 and F3 modules are known (Dickinson *et al.*, 1994; Huber *et al.*, 1994; Sharma *et al.*, 1999; de Pereda *et al.*, 1999; Wah *et al.*, 2002). We have crystallized the ^{2}F1^{3}F1 protein (90 residues, 10.1 kDa) in both the native state and in complex with part of an FnBP from *S. aureus* (STATT1; residues 531–549 of mature FnBPA from *S. aureus*).

2. Expression and purification of the ^{2}F1^{3}F1 module pair

^{2}F1^{3}F1 was expressed and purified as described previously (Schwarz-Linek *et al.*, 2003). The STATT1 peptide was purchased from Alta Bioscience (Birmingham, England).

3. Crystallization of the ^{2}F1^{3}F1 module pair

Initial crystallization screens were performed using a Genesis Pro-Team 150 robot (Tecan) as sitting-drop experiments at 298 K and five commercial screens (Crystal Screens 1 and 2, PEG/Ion Screen, Grid Screen Ammonium Sulfate and Grid Screen Sodium Chloride, all from Hampton Research, USA). A total of 768 conditions were tested by combining 0.2 µl of ^{2}F1^{3}F1 or 0.2 µl of ^{2}F1^{3}F1–STATT1 complex [20 mg ml^{-1} of ^{2}F1^{3}F1 in water (residues 62–151 from the mature human fibronectin) or 20 mg ml^{-1} of ^{2}F1^{3}F1 plus STATT1 in a 1:2 ratio in water] with 0.2 µl of precipitating solution per well. Experiments were monitored every 48 h for 20 d. Crystals were obtained in several conditions containing ammonium sulfate, PEGs of different molecular weights and with a pH between 4 and 5 (Fig. 1*a*). Subsets of these conditions were scaled up to a total volume of 6 µl in hanging-drop experiments, varying the ^{2}F1^{3}F1:STATT1 ratios, protein and precipitant concentration and the pH (Fig. 1*b*). After one month, the original crystallization screens resulted in protein crystals from a new condition: 4 *M* sodium formate, which also conveniently acts as a cryoprotectant solution. Thus, the crystals can be flash-cooled straight from their growth drop.

Previous attempts to determine the structure of the ^{4}F1^{5}F1 module pair failed because all the crystals obtained were perfectly merohedrally twinned (Murray & Garman, 2002). The use of MDP (2-methyl-2,4-pentanediol), glycerol, dioxane *etc.* has been proposed for the avoidance of twinning (McPherson *et al.*, 1986; Bergfors, 1999; CCP4 Bulletin Board, http://

www.ccp4.ac.uk/ccp4bb.html); therefore, addition of these compounds to the mother liquor for crystal growth was tested in the following ranges: 1–2%(*v/v*) MPD and dioxane and 1–10%(*v/v*) glycerol.

The best crystals were obtained using 3 µl of protein solution at 7 mg ml^{-1} in 0.1 *M* sodium acetate pH 4.5, mixed with 3 µl 0.2 *M* ammonium sulfate, 0.1 *M* sodium acetate pH 4.5, 2% MPD and 5% PEG MME 550 at room temperature (condition I; Fig. 1*c*) and using 3 µl of protein solution at 10 mg ml^{-1} in 4 *M* sodium formate (condition II; Fig. 1*d*). In both cases, the addition of STATT1 in a 2:1 ratio (FnBP:^{2}F1^{3}F1) also generates the same crystal shapes and apparent symmetry in sitting-drop or hanging-drop experiments. The crystals grown in condition II only diffracted to 3.2 Å, whereas those from condition I diffracted to better than 1.7 Å. Thus, the latter crystals were used for all but one of the data sets collected.

Prior to data collection, the crystals were either transferred to a cryoprotectant solution obtained by replacing water in the mother liquor with 35%(*v/v*) PEG MME 550 (condition I) or flash-cooled straight from the mother liquor (condition II). Crystals were mounted in plastic cryoloops (Litho-loops, Molecular Dimensions) and flash-

cooled in a 100 K nitrogen stream generated by a 700 Series Oxford Cryostream. In the case of the heavy-atom derivatives (using crystals grown in condition I), the crystals were previously soaked (24–48 h) in their mother-liquor solution plus 10 m*M* K$_2$PtCl$_2$, K$_2$PtCl$_6$, HgCl$_2$, Pb(NO$_3$)$_2$, K$_2$OsCl$_6$, NaAuCl$_4$ or Y$_2$O$_3$ at 298 K. Prior to data collection, the crystals were soaked in cryoprotectant containing no heavy atoms in order to back-soak any non-specifically bound metal out of the solvent channels.

4. Data collection

The crystals were evaluated in-house at 285 and 100 K using a Rigaku rotating-anode source operating at 55 kV and 75 mA fitted with an Osmic blue optic and a MAR 345 imaging-plate area detector. Six data sets were collected at 100 K using the rotating-anode source: three native, two ^{2}F1^{3}F1–STATT1 complex and one K$_2$PtCl$_4$ derivative. Additionally, six further data sets from uncomplexed crystals were collected using synchrotron sources: two native, one at beamline ID14-4 of the European Synchrotron Radiation Facility (ESRF, Grenoble, France) and the other at station 9.6 of the Synchrotron Radiation Source (SRS, Daresbury, England) and two K$_2$PtCl$_6$
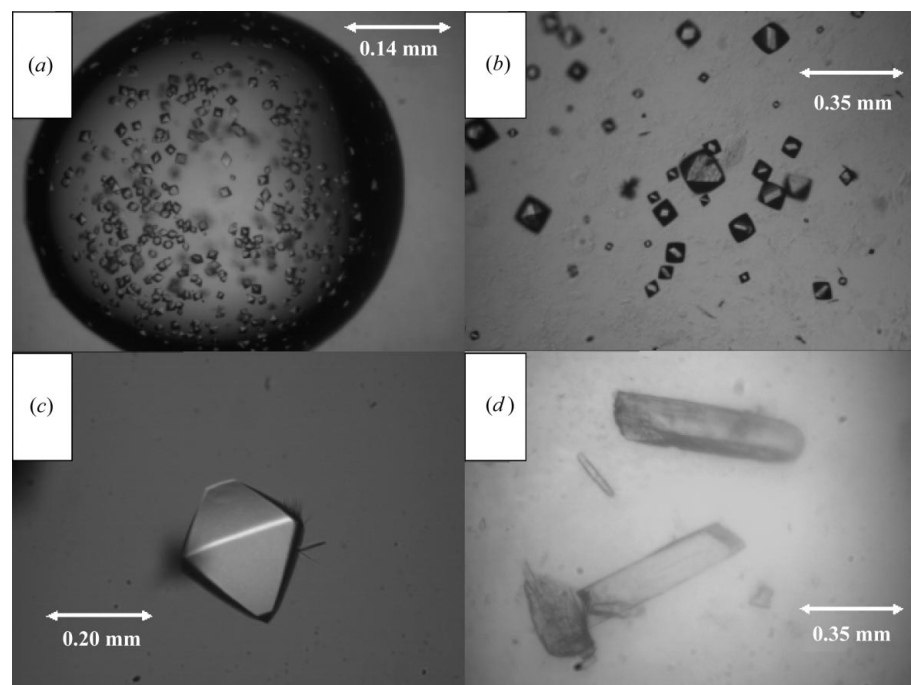

Figure 1
^{2}F1^{3}F1 crystals obtained using the following conditions: (*a*) 0.2 *M* ammonium sulfate, 0.1 *M* sodium acetate pH 4.6, 25% PEG 4000, 0.4 µl drop size using the sitting-drop method; (*b*) 0.2 *M* ammonium sulfate, 0.1 *M* sodium acetate pH 4.5, 5% PEG MME 550, 6.0 µl drop size using the hanging-drop method; (*c*) 0.2 *M* ammonium sulfate, 0.1 *M* sodium acetate pH 4.5, 2% MPD, 5% PEG MME 550, 6.0 µl drop size using the hanging-drop method (condition I); (*d*) 4 *M* sodium formate, 6.0 µl drop size using the hanging-drop method (condition II).

Table 1
MOSFLM autoindexing from data set Native 3.

No.	Penalty	Lattice	Unit-cell parameters						Possible space groups
			a (Å)	b (Å)	c (Å)	α (°)	β (°)	γ (°)	
13	88	hP	37.38	37.38	108.23	90	90	120	$P3$, $P3_1$, $P3_2$ etc.
12	87	oC	37.68	83.80	108.00	90	90	90	$C222$, $C222_1$
11	87	mC	84.06	37.49	108.12	90	89.95	90	$C2$
10	2	tP	37.50	37.50	108.10	90	90	90	$P4$, $P4_1$, $P4_2$, $P4_3$ etc.
9	1	mC	53.06	52.99	108.15	90	90.01	90	$C2$
8	1	oC	52.99	53.06	108.15	90	90	90	$C222$, $C222_1$
7	1	mC	53.01	53.05	108.15	90	89.95	90	$C2$
6	1	mP	37.53	37.48	108.14	90	89.95	90	$P2$, $P2_1$
5	1	oP	37.48	37.53	108.13	90	90	90	$P222$, $P222_1$, $P2_12_12$ etc.
4	1	mP	37.48	37.53	108.14	90	89.97	90	$P2$, $P2_1$
3	0	mP	37.48	108.15	37.52	90	90.08	90	$P2$, $P2_1$
2	0	aP	37.48	37.53	108.15	90.06	89.97	89.94	$P1$
1	0	aP	37.48	37.53	108.15	89.94	89.97	90.06	$P1$

derivatives, one HgCl$_2$ and one Pb(NO$_3$)$_2$ derivative, also at SRS station 9.6. Diffraction images were integrated using *MOSFLM* (Leslie, 1992) and scaling was performed with *SCALA* from the *CCP*4 (Collaborative Computational Project, Number 4, 1994) suite. The crystals were tetragonal (most probable space groups $P42_12$, $P4_12_12$ and $P4_32_12$), with unit-cell parameters $a = b = 37$, $c = 108$ Å, $\alpha = \beta = \gamma = 90°$ (condition I). A Matthews coefficient calculation suggested that there was one molecule per asymmetric unit ($V_M = 1.91$ Å^3 Da^{-1}, with 35% solvent content). The crystals that grew in 4 M

sodium formate (condition II) had unit-cell parameters $a = b = 101.6$, $c = 51.0$ Å, $\alpha = \beta = \gamma = 90°$. These crystals also present 422 symmetry and the unit cell allows space for one ($V_M = 5.55$ Å^3 Da^{-1}, 78% solvent content), two ($V_M = 2.77$ Å^3 Da^{-1}, 56% solvent content) or even three molecules per asymmetric unit ($V_M = 1.85$ Å^3 Da^{-1}, 34% solvent content), the latter two possibilities being more likely.

5. Discussion

Several tests were performed because of the previous experience of twinning in crystals of the ^{4}F1^{5}F1 pair (Pilka, Murray & Garman, 2003). The *MOSFLM* (Leslie, 1992) autoindexing shows in all cases a clear gap from penalty values of close to 90 to 2 in the tetragonal space groups, presenting in addition several monoclinic, orthorhombic and triclinic probable space groups with penalties of 1 or less (Table 1). The R_{merge} statistics or the number of rejected reflec-
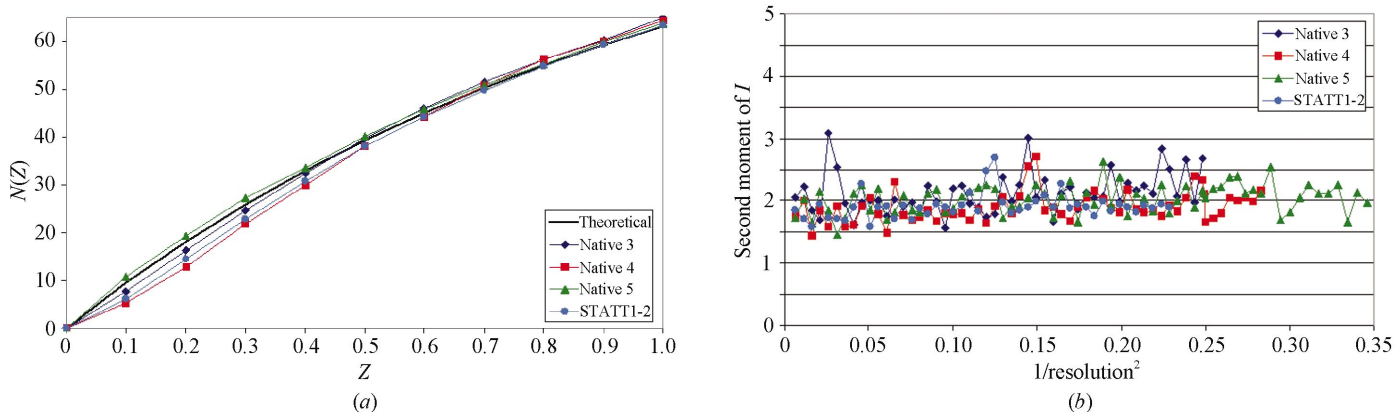
Figure 2
(*a*) Graphical representation of the acentric cumulative distribution function $N(Z)$ relative to Z (where Z is the intensity relative to the mean intensity) and (*b*) second moment of I relative to resolution. Both were calculated using the program *TRUNCATE* (*CCP*4) for data sets Native 3, Native 4, Native 5 and STATT1-2 (see Table 2). In the case of a twinned system, the acentric cumulative distribution would show a clear sigmoidal shape, which is not evident here, and the average value of the second moment of I would be 1.5, whereas the average here is ~2. In (*a*) Theoretical refers to the shape of a non-twinned data set.
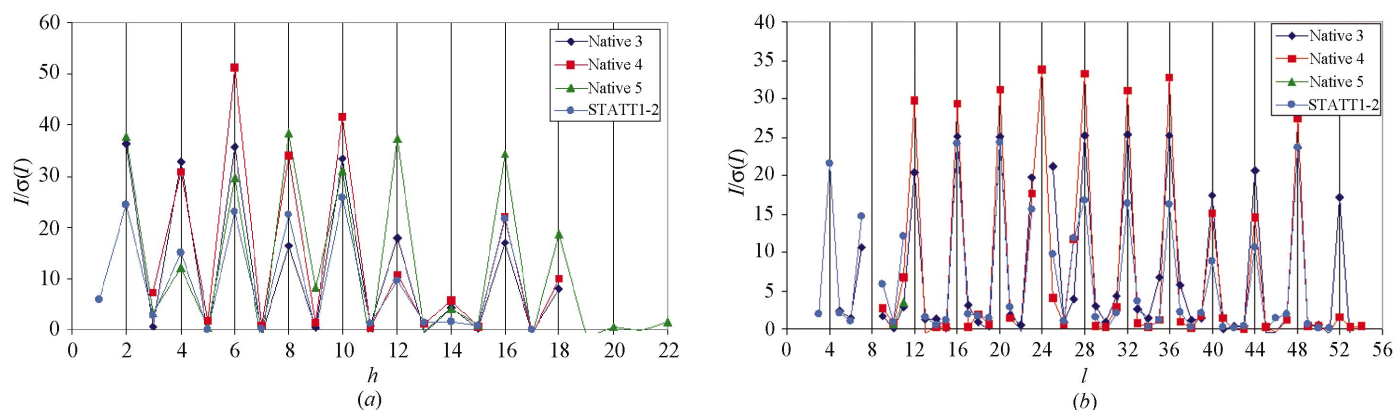
Figure 3
Axial reflections of data sets Native 3, Native 4, Native 5 and STATT1-2 plotted against $I/\sigma(I)$; in (*a*) $h00$ reflections occur at $h = 2n$ and in (*b*) $00l$ reflections seem to occur at $l = 4n$. If $h00 = 2n$ and $00l = 4n$, there are two possible sets of screw rotation axes in the crystal: 2_1 or 4_2 and 4_1 or 4_3.

tions cannot be used to discriminate between the space-group assignments. If the data are integrated in tetragonal space groups belonging to the 4/m Laue class, the merohedral crystal-twinning server (http://www.doe-mbi.ucla.edu/Services/Twinning/; Yeates, 1997) found a consistent twinning fraction of between 0.44 and 0.49. However, for the probable space groups none of the moments of the intensity distributions, the Britton plots or the Yeates $S(H)$ plots (*TRUNCATE* and *DETWIN* in *CCP*4) are indicative of twinned crystals (for tetragonal space groups in the 4/m Laue class). Additionally, the acentric Wilson cumulative distribution does not show the clear sigmoidal shape characteristic of merohedral twinned crystals, nor does the second moment on I (*TRUNCATE* in *CCP*4; Fig. 2). It has recently been shown (Padilla & Yeates, 2003) that most of the previous methods for the detection of twinning may fail in cases of anisotropy, pseudo-non-crystallographic symmetries or pseudo-centring. Padilla & Yeates (2003) proposed a new approach based on differences between local pairs of reflection intensities and separate normalization, which seems to give less ambiguous results. The test gives two quantities, $\langle|L|\rangle$ and $\langle L^2\rangle$, where L is defined

as $[I(h_1) - I(h_2)]/[I(h_1) + I(h_2)]$ and $I(h_1)$ and $I(h_2)$ are the intensities of the unrelated reflections h_1 and h_2. For an untwinned crystal $\langle|L|\rangle = 0.500$ and $\langle L^2\rangle = 0.333$, whereas for a perfectly twinned crystal $\langle|L|\rangle = 0.375$ and $\langle L^2\rangle = 0.200$. This approach, implemented in *DATAMAN* v.6.3 or above (*RAVE*, Uppsala Software Factory), gave us a clear indication of the untwinned nature of our system, since we obtained $\langle|L|\rangle = 0.499$ and $\langle L^2\rangle = 0.330$ using data integrated in $P4$ or in $P422$ from data sets Native 3 and Native 5.

Of all the probable space groups, those in the tetragonal 4/mmm Laue group present the highest symmetry. If the data are integrated in space group $P422$, two screw-rotation axes are clearly present in the I (intensity) *versus* axial reflection plot (Fig. 3), pointing to an enantiomorphic space-group pair: $P4_12_12$ or $P4_32_12$. Note that a plot of $I/\sigma(I)$ against axial reflections did not give such a clean systematic signal, particularly in the 00l reflections, pointing instead to a $P42_12$ space group. A self-rotation function (*POLARRFN*; *CCP*4) shows the presence of two strong peaks: a fourfold axis along the c axis ($\varphi = 90$, $\omega = 90$, $\kappa = 90°$) and a twofold axis along the crystallographic a (or b) axis ($\varphi = 90$, $\omega = 90$, $\kappa = 180°$; Fig. 4).

Additionally, there are twofold peaks every 45° in the ab plane, all supporting a $P422$ space group. In the self-rotation function, no peaks indicating clear non-crystallographic symmetry or twinning operators were found.

Once the most probable space groups had been selected ($P42_12$, $P4_12_12$ and $P4_32_12$), a molecular-replacement approach was attempted using data sets Native 3, Native 5 and STATT1-2 (see Table 2), which were all collected from crystals grown under condition I. For each of the selected space groups, the programs *CNS* (Brünger *et al.*, 1998), *MOLREP* (Vagin & Teplyakov, 1997), *BEAST* and *PHASER* (Read, 2001) were used, with 32 search models: the ^{2}F1 domain average NMR models from PDB codes 1qgb (24 models in total) and 1o9a (15 models in total) and also the first individual 15 NMR models of both of them. No significant solutions were found with any of the tested models, data sets or space groups. This result suggested that the ^{2}F1^{3}F1 pair may have a slightly different structure or that the incomplete model used is not sufficient to detect a clear solution in the rotation and translation lists. We are now trying to solve the structure by SAD, MIR and MIRAS methods. Currently, the heavy-atom search process using space groups $P4_12_12$ or $P4_32_12$

Table 2
Diffraction data statistics.

Values for the highest resolution shell are shown in parentheses. All except STATT1-1 are data collected from crystals grown under condition I.

(*a*) Native or peptide-bound crystals.

	Native 1	Native 2	Native 3	Native 4	Native 5	STATT1-1	STATT1-2
Space group	$P422$	$P422$	$P422$	$P422$	$P422$	$P422$	$P422$
$a = b$ (Å)	37.0	37.0	37.5	37.3	37.4	101.6	37.2
c (Å)	107.3	107.5	108.1	108.1	109.6	51.0	108.1
X-ray source	In-house	In-house	In-house	SRS 9.6	ESRF 14-4	In-house	In-house
Wavelength	1.54179	1.54179	1.54179	0.8700	0.9763	1.54179	1.54179
Resolution range (Å)	30–2.50	30–2.50	30–2.05	30–1.88	30–1.70	30–3.20	30–2.10
	(2.60–2.50)	(2.60–2.50)	(2.15–2.00)	(1.98–1.88)	(1.80–1.70)	(3.30–3.20)	(2.20–2.10)
Completeness (%)	87.3 (87.3)	100.0 (100.0)	99.9 (99.8)	99.2 (95.9)	99.1 (99.1)	99.9 (99.9)	99.8 (99.8)
Unique reflections	2919	2959	5344	6706	9110	4750	4932
Multiplicity	5.5 (6.2)	5.9 (6.4)	39.2 (39.5)	9.7 (6.7)	13.1 (14.0)	6.0 (6.0)	11.1 (11.5)
$I/\sigma(I)$	10.1 (1.9)	5.7 (2.0)	9.2 (3.4)	6.3 (2.0)	5.4 (2.0)	4.4 (2.0)	8.8 (2.4)
R_{merge}†	0.073 (0.362)	0.085 (0.349)	0.055 (0.235)	0.067 (0.366)	0.061 (0.308)	0.167 (0.377)	0.060 (0.278)

(*b*) Heavy-atom derivatives.

	K_2PtCl_4	K_2PtCl_6-1	K_2PtCl_6-2	$HgCl_2$	$Pb(NO_3)_2$
Space group	$P422$	$P422$	$P422$	$P422$	$P422$
$a = b$ (Å)	38.4	39.7	37.7	37.7	37.4
c (Å)	105.4	101.3	107.9	107.8	107.3
Beamline	In-house	SRS 9.6	SRS 9.6	SRS 9.6	SRS 9.6
Wavelength	1.54179	0.8700	0.8700	0.8700	0.8700
Resolution range (Å)	30–2.90(3.00–2.90)	30–1.91(2.01–1.91)	30–1.8(1.90–1.80)	30–1.9(2.0–1.9)	30–2.00(2.10–2.00)
Completeness (%)	99.9 (99.9)	99.1 (94.1)	100 (100)	98.5 (97.4)	100 (100)
Unique reflections	2045	6726	7822	6595	5688
Multiplicity	21.1 (22.3)	4.8 (3.6)	52.6 (54.9)	7.4 (5.9)	12.9 (13.4)
$I/\sigma(I)$	8.5 (2.7)	10.5 (1.8)	2.2 (6.7)	5.0 (3.4)	7.7 (5.7)
R_{merge}†	0.071 (0.295)	0.061 (0.286)	0.063 (0.299)	0.062 (0.324)	0.066 (0.317)

† $R_{\text{merge}} = \sum_{hkl} \sum_i |I_i(hkl) - \{I(hkl)\}|/\sum_{hkl} \sum_i I_i(hkl)$ and $\{I\}$ represent the diffraction-intensity values of the individual measurements and the corresponding mean values. The summation is over all unique measurements.
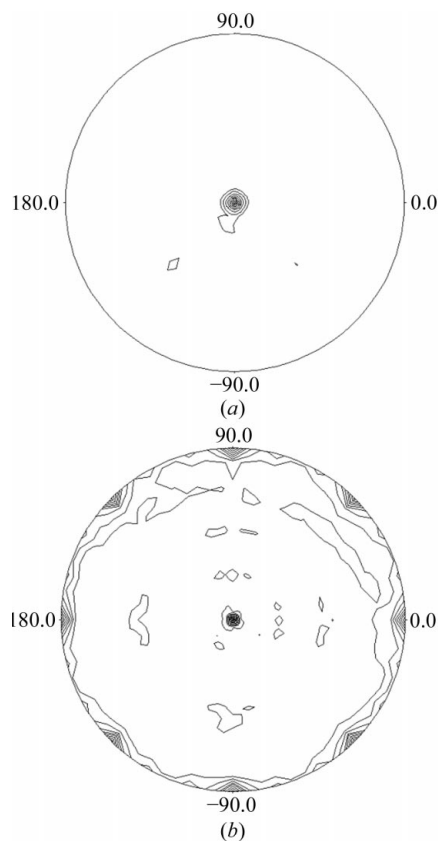
Figure 4
Self-rotation function maps of $^2F1^3F1$ for (a) the $\kappa = 90°$ section and (b) the $\kappa = 180°$ section. Map contouring is at 1σ and was calculated using *POLARRFN* and *xplot84driver* from *CCP4* (data between 30.0 and 2.0 Å resolution from data set Native 3 and integrated in space group $P1$, unit-cell parameters $a = 37.48$, $b = 37.53$, $c = 108.15$ Å, $\alpha = 89.94$, $\beta = 89.97$, $\gamma = 90.06°$).

has found one partially occupied site common to all our derivative-soaked (Pt, Hg and Pb) crystals and two disulfide bridges, but so far there is not enough phasing power to solve the structure.

In the search for heavy-atom binding sites, the relatively low pH at which the crystals were grown (pH 4.5) reduces the probability of finding fully occupied sites. However, in the case of the S atoms (four cysteine and one methionine per F1 module), the very high anomalous multiplicity of some of the data sets has enabled putative sulfur sites to be located, but these have not yet resulted in interpretable electron-density maps. Several of the twinning tests pointed to the non-twinned nature of the system (particularly the Padilla–Yeates method, the second moment of I, the V_M value and the acentric cumulative distribution). However, as a further check, a rotation function of the detwinned data (twinning fraction between 0.42 and 0.48) was calculated in $P4$. These self-rotation functions were the same as those calculated using the original data reduced in $P4$ or $P422$. This result points again to 422 symmetry and a non-twinned system, because the detwinned self-rotation function still exhibited 422 symmetry. The existence of possible non-crystallographic symmetries or pseudo-non-crystallographic symmetries that mimic crystal symmetries is being explored as the most suitable explanation for the pseudo-twinning behaviour in some of the twinning tests.

References

Baron, M., Norman, D., Willis, A. & Campbell, I. D. (1990). *Nature (London)*, **345**, 642–646.

Bergfors, T. M. (1999). Editor. *Protein Crystallization: Techniques, Strategies and Tips*, pp. 226, 245. La Jolla, CA, USA: International University Line.

Bocquier, A. A., Potts, J. R., Pickford, A. R. & Campbell, I. A. (1999). *Struct. Fold. Des.* **7**, 1451–1460.

Bork, P., Downing, A. K., Kieffer, B. & Campbell, I. D. (1996). *Q. Rev. Biophys.* **29**, 119–167.

Brünger, A. T., Adams, P. D., Clore, G. M., DeLano, W. L., Gros, P., Grosse-Kunstleve, R. W., Jiang, J.-S., Kuszewski, J., Nilges, M., Pannu, N. S., Read, R. J., Rice, L. M., Simonson, T. & Warren, G. L. (1998). *Acta Cryst.* D**54**, 905–921.

Collaborative Computational Project, Number 4 (1994). *Acta Cryst.* D**50**, 760–763.

Dickinson, C. D., Veerapandian, B., Dai, X. P., Hamlin, R. C., Xuong, N. H., Ruoslahti, E. & Ely, K. R. (1994). *J. Mol. Biol.* **236**, 1079–1092.

Huber, A. H., Wang, Y. M., Bieber, A. J. & Bjorkmann, P. J. (1994). *Neuron*, **12**, 717–731.

Hynes, R. O. (1990). In *Fibronectins*, edited by A. Rich. Berlin: Springer–Verlag.

Leslie, A. G. W. (1992). *Jnt CCP4/ESF–EACMB Newsl. Protein Crystallogr.* **26**, 27–33.

McPherson, A., Koszelak, S., Axelrod, H., Day, J., Robinson, L., McGrath, M., Williams, R. & Cascio, D. (1986). *J. Cryst. Growth*, **76**, 547–553.

Padilla, J. E. & Yeates, T. O. (2003). *Acta Cryst.* D**59**, 1124–1130.

Pereda, J. M. de, Wiche, G. & Liddington, R. C. (1999). *EMBO J.* **18**, 4087–4095.

Pilka, E. S., Murray, J. W. & Garman, E. F. (2003). Personal communication.

Potts, J. R., Bright, J. R., Bolton, D., Pickford, A. R. & Campbell, I. D. (1999). *Biochemistry*, **38**, 8304–8312.

Potts, J. R. & Campbell, I. D. (1996). *Matrix Biol.* **15**, 313–320.

Read, R. J. (2001). *Acta Cryst.* D**57**, 1373–1382.

Schwarz-Linek, U., Werner, J. M., Pickford, A. R., Gurusiddappa, S., Kim, J. H., Pilka, E. S., Briggs, J. A. G., Gough, T. S., Höök, M., Campbell, I. D. & Potts, J. R. (2003). *Nature (London)*, **423**, 177–180.

Sharma, A., Askari, J. A., Humphries, M. J., Jones, E. Y. & Stuart, D. I. (1999). *EMBO J.* **18**, 1468–1479.

Vagin, A. & Teplyakov, A. (1997). *J. Appl. Cryst.* **30**, 1022–1025.

Wah, D. A., Fernandez-Tornero, C., Sanz, L., Romero, A. & Calvete, J. J. (2002). *Structure*, **10**, 505–514.

Williams, M. J., Phan, I., Harvey, T. S., Rostagno, A., Gold, L. L. & Campbell, I. D. (1994). *J. Mol. Biol.* **235**, 1302–1311.

Yeates, T. O. (1997). *Methods Enzymol.* **276**, 344–358.